Proceedings of the ASME 2011 International Mechanical Engineering Congress & Exposition
IMECE2011
November 11-17, 2011, Denver, Colorado, USA

IMECE2011-62703

EXPERIMENTAL MODAL ANALYSIS OF THE ADVANCED COMBAT HELMET

Alessio Medda
Henry M. Jackson Foundation
Ft. Rucker, AL, USA

Jay Shridharani
Duke University
Durham, NC, USA

Cameron D. Bass
Duke University
Durham, NC, USA

Valeta Carol Chancey
U.S. Army Aeromedical Research Lab.
Ft. Rucker, AL, USA

ABSTRACT

In this work we present a study of the characterization of an Advanced Combat Helmet (ACH) using experimental modal analysis techniques. A medium-sized helmet was impacted at different location and the vibration response was used to estimate a global frequency model. This was achieved using the modal parameters of the local models obtained for a specific input-output location and combining them in a global model. The estimation of the frequency model was done using well-established least squares techniques, while the contribution of measurement noise in input and output was considered.

I. INTRODUCTION

With recent operations in Iraq and Afghanistan, deployed military personnel have experienced an increased incidence of primary, secondary, and tertiary blast effects from near-field blast exposures while performing mounted and dismounted operations. Likewise, an increased prevalence of brain-related injuries, ranging from mild to severe, has been observed. With the recent fielding of the Helmet Mounted Sensor Systems at the direction of the Vice Chief of Staff of the Army, the combat helmet became a key mounting platform for electronic sensor technologies to sense and record dynamic exposures as well as a vital item of personnel protection equipment. To improve combat helmet protection and to understand dynamic exposures measured on helmet mounted sensors, combat helmet mechanical characteristics and dynamic response need to be characterized. The first step in developing this knowledge is to understand the dynamic response of the ACH, which is a complex structure without a readily available computation model to which experimental results could be compared. Traditionally, the study of the dynamic response of a complex structure is a difficult problem to address using solely mathematical and analytical tools, when available finite element models are not available. On the other hand, it is relatively simple to obtain a model that satisfactorily approximates the true dynamics of the structure using experimental techniques. One popular procedure is for the estimation of modal parameters of the system experimental modal analysis. This work focuses on the frequency characterization of the system using the *Frequency Response Function* (*FRF*), defined as the Fourier Transform (FT) of the Impulse Response Function of the system. Given the time histories for a Single-Input-Single-Output (SISO) experiment, least squares optimization methods were used to determine the relations between the input excitation and the output response. The estimated modal parameters were subsequently used to calculate a global *FRF* model of the physical system.

Section II presents a concise outline on the derivation of the *FRF* for a Linear Time Invariant (LTI) system, whereas a detailed account of the results is presented in Section III. A proposed method to generate a global FRF from local FRF measurements is also discussed in section III. Section IV presents the conclusion and future work.

II. ESTIMATION OF THE *FRF* FOR LTI SYSTEMS

In the context of experimental modal analysis, a main classification between time domain identification methods and frequency domain identification methods is underlined in [1] and [2]. In this work, we consider the frequency domain direct method for the estimation of the *FRF* using SISO measurements. If the system can be approximated as a LTI

Report Documentation Page

Form Approved
OMB No. 0704-0188

1. REPORT DATE	2. REPORT TYPE	3. DATES COVERED
NOV 2011		**00-00-2011 to 00-00-2011**

4. TITLE AND SUBTITLE	5a. CONTRACT NUMBER
Experimental Modal Analysis of the Advanced Combat Helmet	5b. GRANT NUMBER
	5c. PROGRAM ELEMENT NUMBER
6. AUTHOR(S)	5d. PROJECT NUMBER
	5e. TASK NUMBER
	5f. WORK UNIT NUMBER
7. PERFORMING ORGANIZATION NAME(S) AND ADDRESS(ES) **U.S. Army Aeromedical Research Laboratory,Fort Rucker,AL,36362**	8. PERFORMING ORGANIZATION REPORT NUMBER
9. SPONSORING/MONITORING AGENCY NAME(S) AND ADDRESS(ES)	10. SPONSOR/MONITOR'S ACRONYM(S)
	11. SPONSOR/MONITOR'S REPORT NUMBER(S)

12. DISTRIBUTION/AVAILABILITY STATEMENT
Approved for public release; distribution unlimited

13. SUPPLEMENTARY NOTES

14. ABSTRACT

In this work we present a study of the characterization of an Advanced Combat Helmet (ACH) using experimental modal analysis techniques. A medium-sized helmet was impacted at different location and the vibration response was used to estimate a global frequency model. This was achieved using the modal parameters of the local models obtained for a specific input-output location and combining them in a global model. The estimation of the frequency model was done using wellestablished least squares techniques, while the contribution of measurement noise in input and output was considered.

15. SUBJECT TERMS

16. SECURITY CLASSIFICATION OF:			17. LIMITATION OF ABSTRACT	18. NUMBER OF PAGES	19a. NAME OF RESPONSIBLE PERSON
a. REPORT	b. ABSTRACT	c. THIS PAGE			
unclassified	**unclassified**	**unclassified**	**Same as Report (SAR)**	**7**	

system, the *FRF* can be derived considering the dynamic equilibrium equation of a multi degree-of-freedom (DOF) system with viscous damping, as following

$$\mathbf{M}\frac{d^2u(t)}{dt^2} + \mathbf{C}\frac{du(t)}{dt} + \mathbf{K}u(t) = f(t) \tag{1}$$

where $\mathbf{M}$ is the mass matrix, $\mathbf{C}$ is the viscous damping matrix and $\mathbf{K}$ is the stiffness matrix. The quantity $u(t)$ is the displacement as a function of time. The homogeneous solution for a single DOF of eq. (1) has the general form

$$u(t) = Ae^{p_1 t} + Be^{p_2 t} \tag{2}$$

where the constants A and B are derived from the initial conditions. In case of under-damped systems, the roots of (2) are always complex conjugate of each other, and take the form

$$p_1 = -\sigma_1 + j\omega_1^d \qquad p_2 = p_1^* = -\sigma_1 - j\omega_1^d \tag{3}$$

where σ_1 is the damping factor, and $\omega_1^d = 2\pi f_1^d$ is the *damped* natural frequency. Also,

$$p_1, p_1^* = -\xi_1\omega_1^n \pm j\omega_1^n\sqrt{1-\xi_1^2} \tag{4}$$

where ξ_1 represents the *damping ratio*, the ratio of actual system damping to the critical system damping, and ω_1^n is the undamped natural frequency. The Impulse Response of the system is obtained considering the system at rest with zero initial conditions and excited by a unit impulse. In this case, the response takes the following form

$$h(t) = e^{\sigma_1 t}\left[Ae^{j\omega_1^d t} + A^* e^{-j\omega_1^d t}\right] \tag{5}$$

Taking the FT of (5) and grouping the common terms we obtain

$$[-\omega^2\mathbf{M} + \omega\mathbf{C} + \mathbf{K}]U(\omega) = F(\omega) \tag{6}$$

Defining $B(\omega) = -\omega^2\mathbf{M} + \omega\mathbf{C} + \mathbf{K}$, then the system response due to a known input is obtained by

$$U(\omega) = \frac{F(\omega)}{B(\omega)} = H(\omega)F(\omega) \tag{7}$$

The complex function $H(\omega)$ is the *FRF*, while $B(\omega)$ is the *characteristic equation* of the system. The characteristic values of $B(\omega)$ are the complex roots of the characteristic equation and are called *modal frequencies*. An often used alternative representation of $H(\omega)$ is the partial fraction form proposed in [3], defined as follows

$$H_{P,Q}(\omega) = \frac{1}{B(\omega)} = \sum_{k=0}^{N_p}\left(\frac{R_k}{j\omega - p_k} + \frac{R_k^*}{j\omega - p_k^*}\right) \tag{8}$$

where N_p is the number of roots of $B(\omega)$ and R_k, R_k^* are the residuals. In (8), the indices in $H_{P,Q}(\omega)$ relate the response at coordinate *P* with the input at coordinate *Q*. This representation allows the direct estimation of the modal parameters directly from the *FRF*, using the following procedure

- Given a set of input-output data for an excitation at position *P* and a response at position *Q*, estimate the *FRF* and the coherence function.
- Isolate the *FRF* peaks, and for each peak
  - The damped natural frequency is the position of the peak in the *FRF* log-magnitude plot.
  - The damping ξ_k is computed as the -3dB bandwidth of the peak, as $\xi_k = \frac{\Delta\omega|_{-3dB}}{2\omega_k^d}$
  - The amplitude of the peak is the quantity $\left|\frac{R_k}{\sigma_k}\right|$

The estimation of the *FRF* from experimental measured data is obtained from the FT of the convolution integral of an LTI system, as

$$H(\omega) = \frac{Y(\omega)}{X(\omega)} \tag{9}$$

where $X(\omega)$ and $Y(\omega)$ are the FT of the input and output vibration signal. In case of noise in the measured signals, the estimated *FRF* is affected by random errors, as highlighted in Fig. 1. To avoid instability in the measurements, the H_1 and H_2 estimators of the *FRF* are defined as

$$H_1(\omega) = \frac{S_{XY}(\omega)}{S_{XX}(\omega)} \qquad H_2(\omega) = \frac{S_{YY}(\omega)}{S_{YX}(\omega)} \tag{10}$$

The quantities S_{YX}, S_{YY}, S_{XX}, and S_{XY} are the FT of the autocorrelation and cross correlation functions $R_{yx}(\tau)$, $R_{yy}(\tau)$, $R_{xx}(\tau)$, and $R_{xy}(\tau)$. In total absence of noise, H_1 and H_2 are equivalent to each other and to $H(\omega)$, as defined in (9). Only if the input is noise-free, the estimator H_1 is equivalent to $H(\omega)$, and only if the output is noise-free the estimator H_2 is equivalent to $H(\omega)$. When noise is present in the input and output measurements at the same time, a different estimator than (10) is required to reduce the bias errors. Many solutions are present in the literature, and one of these solutions is the H_v estimator, which minimizes the effect of errors in the input as well as in the output, assuming that the spectral characteristics of the signals are known [4]. The H_v estimator is defined as

$$H_v(\omega) = \frac{\overline{S_{YY}}(\omega) - \overline{S_{XX}}(\omega) \pm \sqrt{[\overline{S_{XX}}(\omega) - \overline{S_{YY}}(\omega)]^2 + 4|\overline{S_{YX}}(\omega)|}}{2\overline{S_{XY}}(\omega)} \tag{11}$$

In the case that the input and output noise to signal level (SNR) are equivalent to each other and are uncorrelated, the H_v estimator is the geometric mean of the estimators H_1 and H_2. As shown in [5], the use of (11) offers important advantages, as

long as the signal to noise ratio (SNR) is above the 3dB threshold.

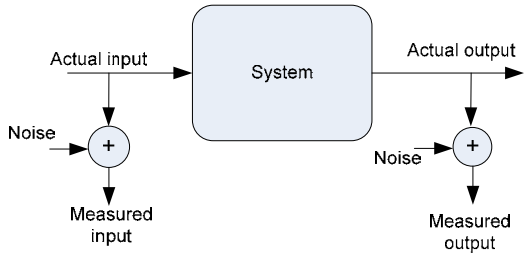

Figure 1 – Contribution of the noise in the measurement of input and output signals.

In many practical applications, because the SNR at the input and output is difficult to measure or not readily available, the coherence function is used instead as a quality measure for the estimated frequency peak. The coherence is defined as

$$\gamma_{XY}^2 = \frac{\left|\overline{S_{XY}}(\omega)\right|^2}{\overline{S_{XX}}(\omega)\overline{S_{YY}}(\omega)} \tag{12}$$

with $\gamma_{XY}^2 \in [0,1]$, and it represents a measure of causality for a given frequency, with perfect causality given by a coherence of 1.

III. EXPERIMENTAL MODAL ANALYSIS ON A MEDIUM SIZE ACH

The data collection for the estimation of the *FRF* model was performed on a medium-sized ACH. Only the helmet shell is used on the test, with the chin straps and retention system removed. The system was isolated using a fishing line to suspend the helmet to a horizontal beam to minimize the effect of the surrounding noise and vibration in the room. The helmet was impacted in various locations with a calibrated impact hammer and the resulting vibration was captured by a tri-axial accelerometer mounted on the crown of the ACH. A picture of the helmet showing the right side shell impact locations and the sensor block is visible in Fig. 2. The impact hammer used is the PCB 086C03 Modally Tuned hammer with mounted hard tip, with a frequency response that decreases to -10 dB at 10 KHz, as shown in Fig. 3.

The helmet was impacted in five locations along the midsagittal and midcoronal line, with five repetitions at each location for a total of 50 tests. The impact locations were marked with the labels MC1 to MC5 and MS1 to MS5, with location MC3 equivalent to location MS3. The helmet was assumed to come to a complete rest after about 2 minutes from the previous impact. The data was collected using a sampling rate of 100 kHz, which provided a usable bandwidth of 50 kHz. An example of the collected signals, along with their power spectrum estimates are reported in Fig. 4 and Fig. 5. These signals were obtained for an impact at location MC2, with the power spectra density computed using the periodogram estimator with a hamming windowing of the data [6]. In Fig. 4, the bandwidth of the impact hammer at -10 dB estimated from the periodogram was consistent with the spectral characteristics of the hammer tip used, resulting in a value of about 4 kHz. After this point, the noise in the signal becomes predominant and the SNR drastically decreases. The 4 kHz mark also defines the usable frequency range in which the modal frequencies are detected. In fact, input-output ratios as defined in equation (9) for frequencies above this value, will model the noise realization and not the signal. To mitigate the effect of the noise on the estimated *FRF*, several solutions were adopted. The signal was filtered using a lowpass digital filter tuned to the bandwidth of the input signal. The filter type was IIR-elliptic with a passband frequency at 3.5 kHz, stopband frequency at 4 kHz, attenuation in the stopband of -80 dB, and ripple in the passband of 0.2 dB. Moreover, in the computation of the autocorrelation and crosscorrelation spectra, both averaging and windowing techniques were used.

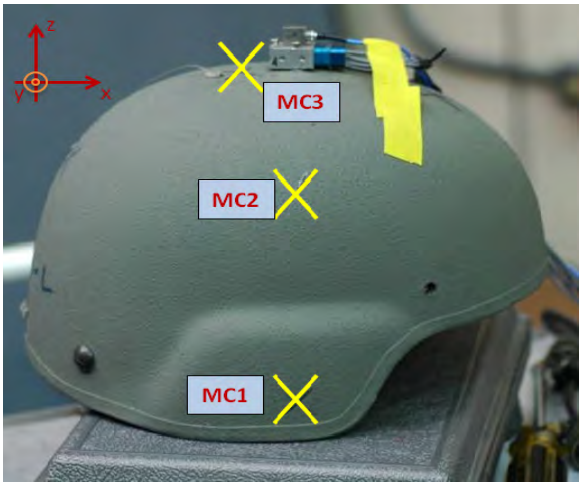

Figure 2 – Picture of the helmet shell with marked impact location and reference system orientation. The sensor block that accommodates the accelerometers and angular rate sensors (not used in this study) was mounted in the crown of the helmet, as visible in the picture.

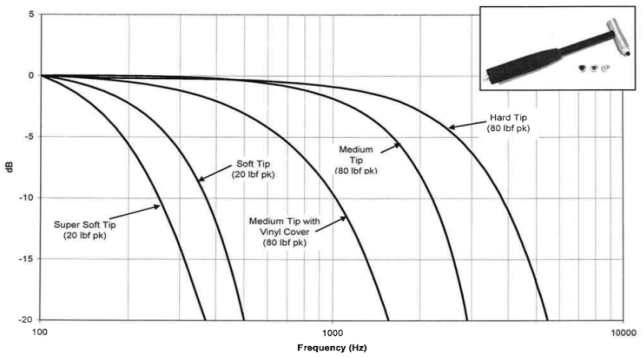

Figure 3 – Frequency response plots of the modally tuned impact hammer PCB 086C03 for different impact tips softness.

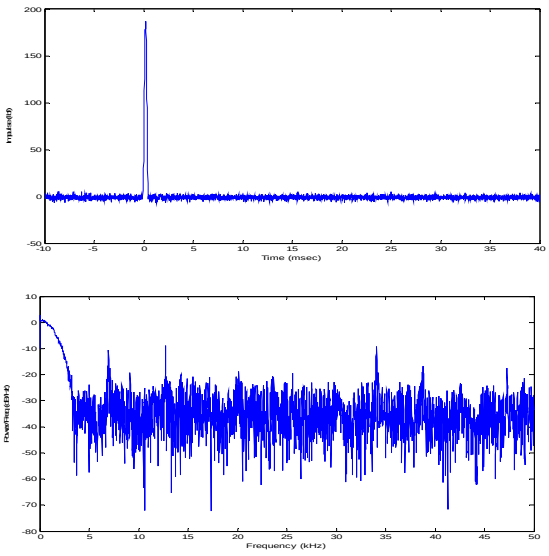

Figure 4 – Impulse hammer signal (top) along with its power spectrum estimate (bottom)

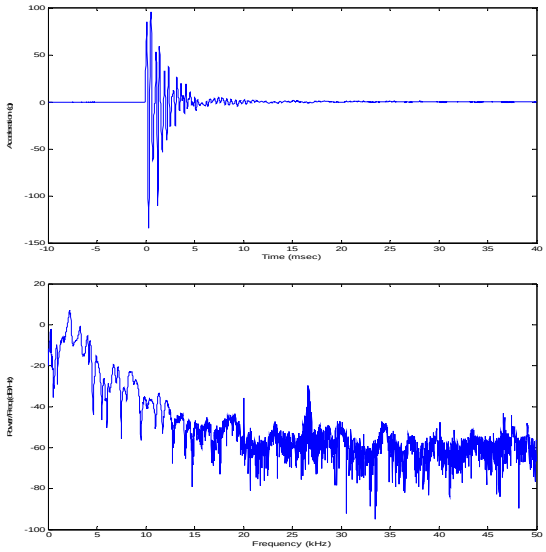

Figure 5 – X-axis vibration response corresponding to the input signal of Fig. 4. The time signal shows acceleration peaks close to 100 g (top), while the power spectrum estimate shows that the power of the signal is concentrated in the first 8 kHz to 10 kHz.

The averaging of the power spectrum is a commonly used technique in experimental modal analysis and it is computed using several repetitions of the same experiment. This procedure is equivalent to the averaging of the single periodograms computed for each repetition, and is generally defined as

$$\overline{S_{AB}}(\omega) = \frac{1}{K}\sum_{i=1}^{K} A_i(\omega)B_i^*(\omega) \qquad (13)$$

where $A(\omega)$ and $B(\omega)$ are the FT of a generic input and output signal, and K represents the number of repetitions for the same experiment; in our case $K = 5$. Moreover, windowing of the signal before the computation of the FT assures that leakage errors are controlled and distortion is minimized. In our analysis, a Hamming window was used.

Figure 5 shows the H_v estimate obtained for location MC2 (crown of the helmet), using five repetitions of the same experiment. The top plot shows the magnitude square of the estimated *FRF* for the three axes, while the bottom plot displays the estimated coherence. A closer analysis of the plots in Fig. 6 reveals the presence of strong peaks up to 1 kHz, a linear increase in power up to about 3 kHz after which begins the incoherent region, where the estimated model follows only the noise realization. For this reason, we limited the frequency resolution to 2.8 kHz. Another phenomenon observed in Fig. 6 is the drops in the coherence function at frequencies consistent with the peaks in the FRF magnitude plot. These characteristic drops are often associated with leakage problems and a deviation from the ideal LTI assumptions. Although measures to reduce leakage were implemented, the problems still persisted, and it is likely linked to nonlinearities in the structure.

Figure 7 to Fig. 9 illustrates the peak picking frequency selection described in Section II for the *x*-, *y*-, and *z*-axis responses. The *FRFs* were estimated from data collected at location MC2, and are the same of those shown in Fig. 6. The peaks of the magnitude response are highlighted with a circle marker on the magnitude response plots, while the correspondent coherence values are highlighted using a square marker on the coherence plots. The coherence values associated with the selected frequencies were used as indication of the quality of the modal frequencies, with a threshold of at least 0.8.

The modal parameters estimated from the curves of Fig. 7 to Fig. 9 are summarized in Table I, where the measured coherence, damping ratios and absolute value of the residuals are also listed. These modal parameters were used to compute an approximate model of the system at location MC2, using the representation in equation (8). The magnitude and phase of the estimated *FRF* for location MC2 are shown in Fig. 10, where the three dominant modes are common among all three coordinates. The modal frequencies associated to these modes are located at circa 300 Hz, 2200 Hz, and 2330 Hz.

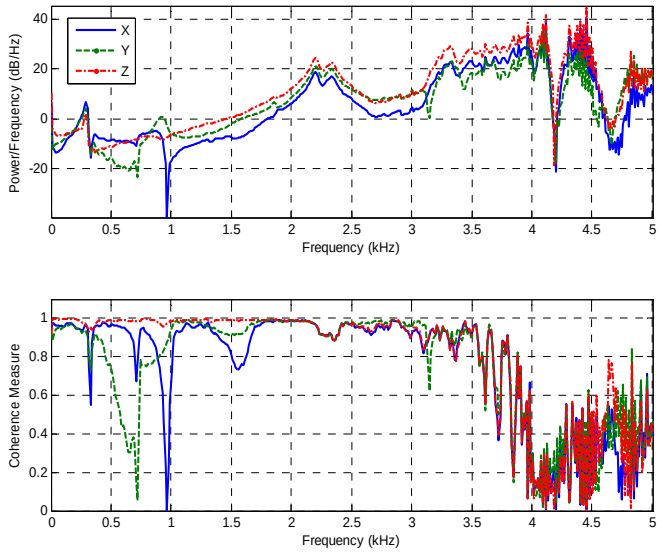

Figure 6 – Estimated *FRFs* for a series of five experiments at location MC2 displaying the magnitude square estimates (top) for the tree linear coordinates and coherence functions (bottom).

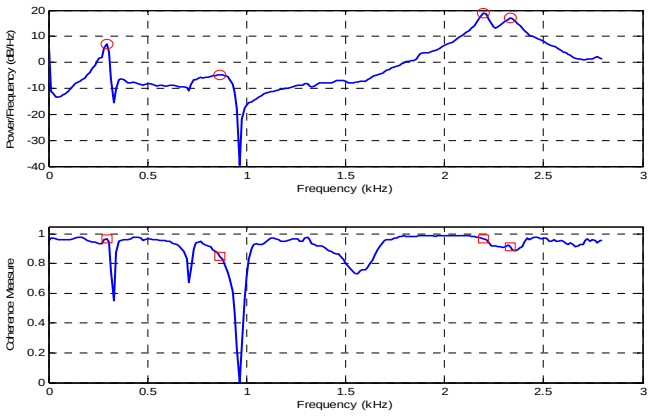

Figure 7 – X-axis FRF peak picking results.

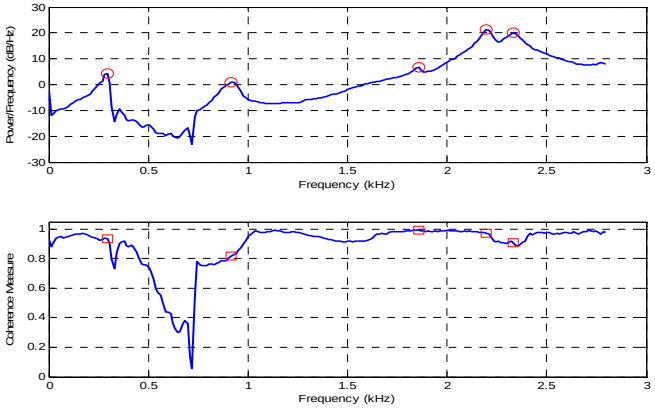

Figure 8 – Y-axis FRF peak picking results.

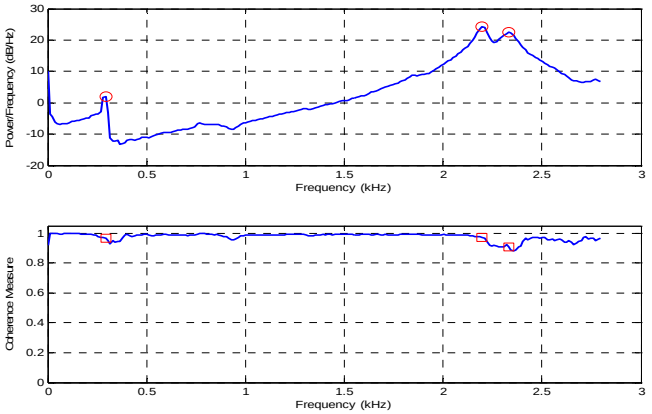

Figure 9 – Z-axis FRF peak picking results.

Table I - Modal Parameters from experimental input-output vibration data at location MC2.

	f (Hz)	Coh	ξ (%)	$\|R\|$
x	293.0	0.97	12.50	2.24
	866.7	0.85	12.68	0.58
	2197.3	0.97	1.67	8.70
	2331.5	0.91	3.05	7.22
y	293.0	0.93	12.50	1.65
	915.5	0.82	13.33	1.12
	1855.5	0.99	1.97	2.16
	2197.3	0.97	1.38	11.50
	2331.5	0.91	2.35	10.04
z	293.0	0.97	33.33	1.25
	2197.3	0.97	1.03	16.50
	2331.5	0.91	1.76	13.49

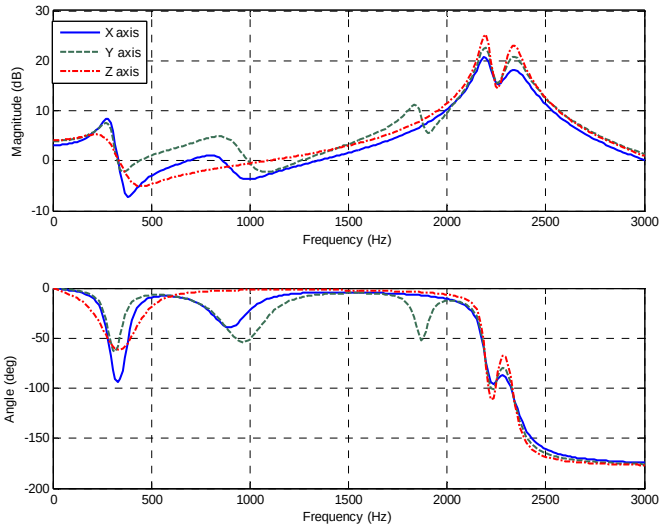

Figure 10 – Partial fraction model for location MC2, computed from the estimated values in Table I. Magnitude and phase are displayed for the *x*, *y*, and *z*-axes.

Derivation of an FRF aggregated model.

The previously described technique was applied to data collected at all 10 locations, from MC1 to MC5 and from MS1 to MS5, where the common crown location MC3 ≡ MS3 is considered twice. A set of *FRFs* was obtained for each location. Each estimated *FRF* model derived from the corresponding modal parameters at a specific location was only representative of the structural response at that location, although similar to the estimated responses at neighbor locations. Observations on the results obtained from this set of *FRFs* shows that some modal frequencies occur at multiple measurement locations, with small changes in amplitude and peak value. This behavior may indicate that we are observing some global modes of the system, rather than local behavioral components. Therefore, it is reasonable to attempt the derivation of a global approximation of the system modal response using these local results. A collective analysis of the estimated modal parameters revealed that 34 modal frequencies were detected for the *x*-coordinate, 35 for the *y*-coordinate, and 28 for the *z*-coordinate. When these frequencies were ordered by increasing value and represented graphically, similar values appeared to be group together, as shown on the plots of Fig. 11.The plots exhibits a staircase profile, with flat zones indicating multiple detection of the same modal frequency. The small difference in amplitude among similar values is representative of small system variation among different locations. In Fig. 11 this concept is highlighted using square boxes to group common values. The mean amplitude of each group is representative of a global modal frequency, with the values of the damping ratio and residual also obtained by averaging the corresponding values in the same group. Table II reports the results of this analysis for the three linear coordinates, while Fig. 12 shows the reconstructed *FRF* models computed from the values in Table II, using equation (8).

Table II – Global modal parameter estimated for the *x*-, *y*- and *z*-coordinate.

x			*y*			*z*		
f (Hz)	ξ (%)	$\|R\|$	f (Hz)	ξ (%)	$\|R\|$	f (Hz)	ξ (%)	$\|R\|$
283.5	0.192	1.94	284.8	0.164	1.82	289.9	0.184	1.33
720.2	0.110	1.01	726.3	0.093	1.46	750.7	0.041	0.93
901.6	0.121	0.81	901.3	0.125	1.32	1293.9	0.030	1.87
1300.0	0.056	1.53	1300.0	0.042	0.97	1916.5	0.243	2.86
1595.0	0.051	0.76	1901.2	0.022	2.01	2221.7	0.017	17.96
2205.4	0.025	9.93	2203.4	0.021	12.91	2390.1	0.017	11.64
2358.0	0.028	6.75	2358.4	0.024	9.36	2502.4	0.005	7.88
			2502.4	0.005	4.91			

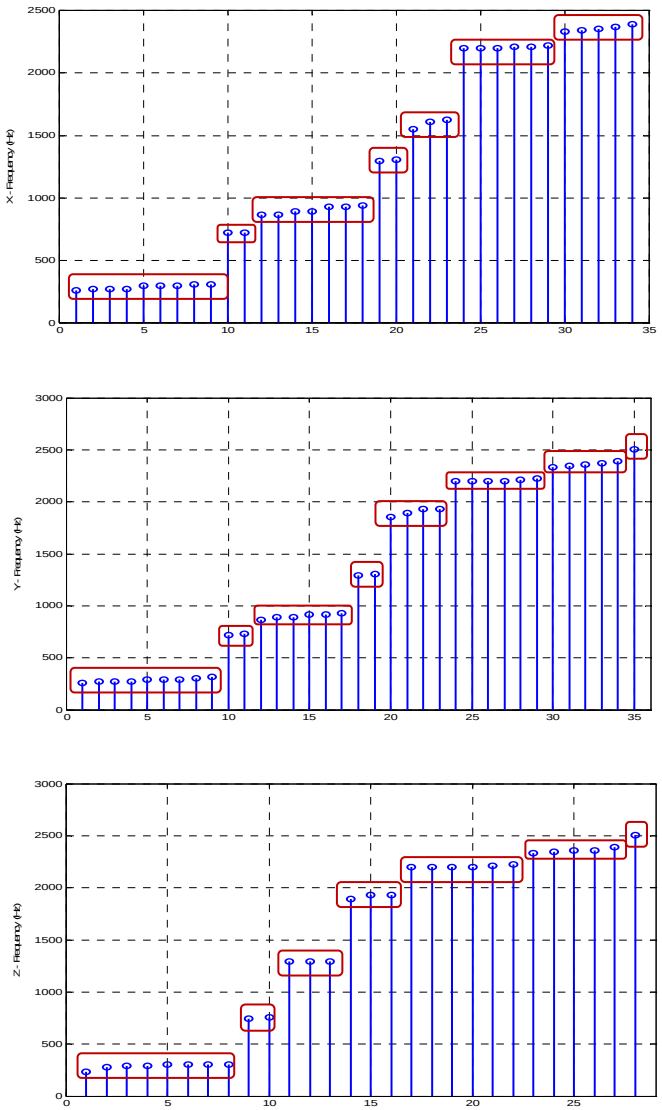

Figure 11 – Ordered collection of detected frequencies for the *x*- (top), *y*- (middle), and *z*-coordinate (bottom). The profile of the plot indicates modes common to multiple locations.

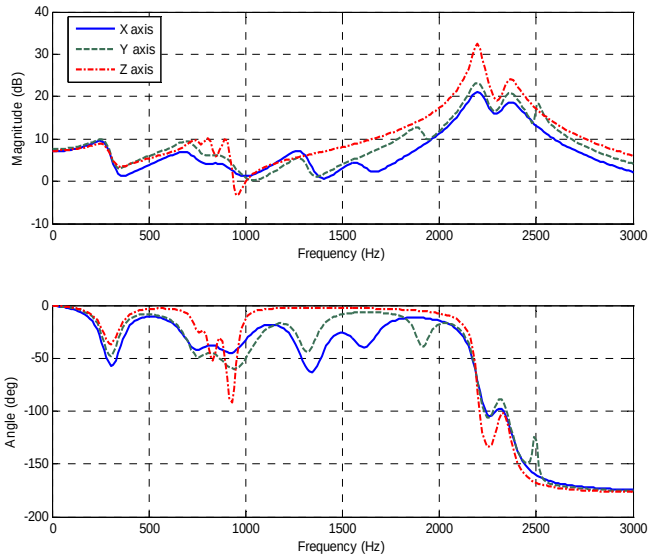

Figure 12 – Global partial fraction model for the collective frequencies of Tab. II. The peaks of the magnitude response (top) align well, identifying global modes for the system.

IV. CONCLUSIONS

In this work we developed a global frequency-based model for a medium-sized ACH based on the *FRF* estimated at multiple locations along the shell of the helmet. The *FRF* estimation was conducted using input-output experimental modal analysis data and employing an estimator that accounts for noise error in the input and output signals. It was found that although different modal frequencies were estimated at different locations, when parameters from all locations were considered, some values can be group together. These frequencies exhibited similar amplitude with similar 3dB bandwidths, therefore were believed to represent global modes of the system. The resulting averaged global parameters were used to derive an aggregate model representative of the dynamic behavior of the ACH. These models exhibited higher energy for the higher frequency modes than the lower frequency ones. This is an unusual behavior, as it is believed that the lower frequency modes retained the majority of the energy of the system. It is suspected that this behavior was associated with the coupling of the sensor mounting block with the helmet, producing unwanted resonances in the frequency range of interest. This behavior, along with the dynamic characterization of the mounting block needs to be investigated further in future studies.

DISCLAIMER

The views, opinions, and/or findings contained in this report are those of the authors and should not be construed as an official Department of the Army position, policy, or decision, unless so designated by other official documentation. Citation of trade names in this report does not constitute an official Department of the Army endorsement or approval of the use of such commercial items.

REFERENCES

[1] Lieven, N. A. J. and Ewins, D. J., 2001, “The Context of Experimental Modal Analysis,” Phil. Trans. R. Soc. Lond., **359**(1778), pp. 5-10.

[2] Maia, N. M. M. and Silva, J. M. M., 2001, “Modal Analysis Identification Techniques,” Phil. Trans. R. Soc. Lond., **359**(1778), pp. 29-40.

[3] Richardson, M. H. and Formenti, D. L., 1982, “Parameter estimation from frequency measurements using rational fraction polynomials,” Proc. 1st Int. Modal Anal. Conf., pp. 167-181.

[4] Hammond, J. K. and Waters, T. P., 2001, “Signal Processing for experimental modal analysis,” Phil. Trans. R. Soc. Lond., **359**(1778), pp. 41-59.

[5] Schoukens, J. and Pintelon, R., 1990, “Measurement of frequency response functions in noisy environments,” IEEE Trans. Instrum. Meas. **39**(6), pp. 905-909.

[6] Hayes, Monson H., Statistical Digital Signal Processing and Modeling, Wiley & Sons.